



26 **INTRODUCTION**

27 Hollowcore slabs are precast/prestressed concrete elements that are commonly used in the  
28 construction industry. They are manufactured at a precast concrete plant prior to shipping to the  
29 job site. After installation, they are typically topped with a 50 mm cast-in-place concrete topping  
30 to level the surface. Structural engineers can make use of the concrete topping to increase the  
31 load carrying capacity of the slab. This consideration requires that failure at the interface  
32 between the hollowcore slab and the concrete topping does not initiate prior to reaching the  
33 ultimate capacity of the composite section. North American design standards specify that the  
34 shear strength of the interface between intentionally roughened hollowcore slab surface and the  
35 concrete topping can be taken as 0.70 MPa, CSA A23.3-04<sup>1</sup> clause 17.4.3.2, or 0.55 MPa, ACI  
36 318-08<sup>2</sup> clause 17.5.3.1. ACI 318-08 commentary clause R17.5.3.3 defines “intentionally  
37 roughened” as a 6.4 mm of surface roughness and CSA A23.3-04 explanatory note N17.4.3.2<sup>1</sup>  
38 defines it as roughness to amplitude of 5.0 mm. In North America, hollowcore slabs are  
39 commonly produced using the extrusion process, which involves the use of zero-slump concrete  
40 mix and high vibration augers. The surface of hollowcore slabs manufactured using this process  
41 is referred to as “machine-cast-finish”. The roughness of this surface varies depending on  
42 number of factors including: concrete mix design and wear and tear of the concrete extrusion  
43 machine. The same variability exists when this surface is roughened. Roughening a hollowcore  
44 slab surface to the amplitudes specified in the design standards involves additional time, material  
45 and labor that manufacturers would be keen to avoid. A simple roughening technique that is  
46 widely used by manufacturers involves the use of a steel broom. However, the produced  
47 roughness does not qualify the slabs to be ranked as “intentionally roughened”.

48

49 The shear strength provided at the interface between hollowcore slabs and the concrete topping  
50 was investigated using full-scale tests for different surface finishes<sup>3, 4</sup>. The test results provided  
51 evidence that horizontal shear levels given in ACI 318<sup>2</sup> are highly conservative. Girhammar and  
52 Pajari (2008)<sup>5</sup> reported that the composite action increases the shear capacity of hollowcore slabs  
53 by 35%. Ibrahim and Elliot (2006)<sup>6</sup> studied the horizontal shear along the interface between  
54 hollowcore slabs and concrete topping for smooth and roughened specimens. Roughness was  
55 achieved using a steel wire brush. Moisture condition of the slab specimens before casting of the  
56 concrete topping was also a factor in the study. The study evaluated the shear capacity of the  
57 composite slabs using push-off tests. It was concluded that the roughness of the slabs was not  
58 significant to differentiate between “smooth” and “roughened” surfaces. However, surface  
59 moisture condition considerably affected the results, where dry and ponded surfaces achieved  
60 lower values compared with the wet surfaces.

61  
62 This paper investigates the shear and peel behavior at the interface between hollowcore slabs and  
63 cast-in-situ concrete topping through four push-off tests. The tested hollowcore slabs have  
64 roughened surface finish. The paper then models the shear and peel stresses along the interface  
65 between the hollowcore slab specimen and the concrete topping. The model is based on the  
66 technique presented by El Damatty and Abushagur<sup>7</sup> to calculate the shear and peel stresses in the  
67 adhesive attaching FRP sheets to the flanges of steel I beams. A closed form solution of the  
68 system equilibrium was used to determine the distribution of the developed shear and peel  
69 stresses.

70 .

71

72

73 **EXPERIMENTAL PROGRAM**

74 Four 1219 mm by 1219 mm by 203 mm thick hollowcore slabs obtained from two manufacturers  
75 (A, B) were tested. Their surfaces were roughened using a conventional steel broom as shown in  
76 Fig. 1a. The depth of the produced random grooves was about 1 mm and each manufacturer had  
77 its own pattern as shown in Figs. 1b and 1c.

78

79 The manufacturer specified concrete compressive strength was 41 MPa. Fig. 2 shows 50 mm  
80 cubes that were sampled from the edges of each slab. Testing these cubes according to ASTM  
81 C349<sup>9</sup> and calculating the equivalent average cylinder concrete compressive strength showed that  
82 the actual strength was 53 MPa and 58 MPa for slabs from manufacturer A and B, respectively.  
83 Each of the tested slabs had four-½” prestressing strands.

84

85 The concrete topping properties were chosen to simulate general practice for this type of  
86 construction. Its thickness was 50 mm and it covered an area of 508 mm by 508 mm. The  
87 surfaces of the hollowcore slabs were wetted and then left to dry to obtain a “saturated dry  
88 surface” condition before casting of the topping. This prevented the water of the concrete  
89 topping to infiltrate into the hollowcore slab surface and produce a weak interface surface. The  
90 concrete mix was provided by a ready mix manufacturer and contained 10 mm pea stone  
91 aggregates and normal Portland cement. Neither air entraining agents nor additives were used.  
92 The measured average slump was 120 mm. The concrete topping did not contain any reinforcing  
93 bars to match the industry practice. Formwork and casting of the concrete topping are illustrated  
94 in Figs. 3a and 3b. Curing was done according to CSA A23.1-09<sup>8</sup> for class “N” exposure by wet

95 curing for three days in the laboratory environment. Three concrete cylinders were tested  
96 according to ASTM C39<sup>10</sup> to evaluate the compressive strength of the concrete topping on the  
97 day of the push-off tests. The average strength was found to be 30 MPa.

98

### 99 **Push-off Tests**

100 The push-off tests were conducted in the vertical orientation. Fig. 4a shows a schematic of the  
101 test setup where the hollowcore slab was installed in the vertical direction with the concrete  
102 topping resting on 50 mm thick steel plate. The shear force was applied by the MTS hydraulic  
103 actuator on a spreader steel beam that pushed the hollowcore slab specimen downward. The steel  
104 plate reacted by a force on the concrete topping. This force generated shear and peel stresses  
105 along the interface between the hollowcore slab and the topping. The steel frame positioned in  
106 the back of the hollowcore specimen was designed to prevent the overturning of the test  
107 specimen. The soffit of the hollowcore slab specimen was sufficiently smooth to allow free  
108 movement of the steel frame without providing additional resistance. 50 mm wide by 3.2 mm  
109 thick Korolath brand bearing pads were used under the steel spreader beam and between the steel  
110 plate and the concrete topping to guarantee a uniform stress distribution at those locations. Fig.  
111 4b shows a photo of the final test setup.

112

113 To capture the state of strains in the concrete topping, strain gauges were attached to its top  
114 surface as illustrated in Fig. 5. Three strain gauges (S1, S3, and S5) were installed along the  
115 vertical centerline to measure strains in the direction of the applied load. Strain gauges S2 and S4  
116 were installed to evaluate the stress distribution across the width of the slab. The push-off tests  
117 induced two types of stresses on the interface between the concrete topping and the hollowcore

118 slab: shear and peel stresses. Four Linear Variable Displacement Transducers (LVDTs) were  
119 used to measure movements in the shear (L3 and L4) and peel (L1 and L2) directions. LVDTs  
120 (L3 and L4) were attached to the hollowcore slab with their armatures resting on angle brackets  
121 attached to the side of the concrete topping. This setup allowed LVDTs to read the differential  
122 displacement between the hollowcore slab and the concrete topping.

123

124 Prior to starting the test, a careful visual inspection did not reveal any signs of separation  
125 between the concrete topping and the hollowcore slabs. The load was applied via the hydraulic  
126 actuator at a rate of 10 kN/minute. Displacement and strain readings were collected throughout  
127 the tests.

128

## 129 **Test Results and Discussion**

130 The ultimate load, at which the concrete topping separates from the hollowcore slab, and the  
131 corresponding average shear strength,  $v_{h \text{ avg.}}$ , are shown in Table 1. To obtain a conservative  
132 estimate of  $v_{h \text{ avg.}}$ , the effect of slippage on the contact area was not accounted for and, thus,  $v_{h \text{ avg.}}$   
133 was directly calculated by dividing the failure load by the contact area. The ultimate load  
134 accounts for the weight of the slab and the steel spreader beam. The average horizontal shear  
135 strength for all of the tested slabs was higher than the limit of 0.7 MPa and 0.55 MPa required by  
136 CSA A23.3<sup>1</sup> and ACI 318<sup>2</sup>, respectively. Slabs from manufacturer A (slabs A1 and A2)  
137 demonstrated considerably higher shear strength than those from manufacturer B (slabs B1 and  
138 B2). This difference might be due to the initial surface roughness and/or the roughening pattern.

139

140 Strains recorded by S2, S3 and S4 showed close agreement in terms of values and trends as  
141 illustrated in Fig. 6 considering slab A1. Slight misalignment of the strain gauges with the load  
142 direction might have led to the shown differences. This close agreement indicates that the  
143 stresses were uniform across the slab width. Extremely brittle and abrupt failure was observed  
144 for all of the tested specimens. Load versus slip curves are shown in Fig. 7. The slip values  
145 represent the average reading of LVDTs L3 and L4. The maximum difference between the  
146 readings of LVDTs L3 and L4 was less than 10% for all slabs. The curves generally illustrate  
147 two stages; pre-yielding stage where the slope is considerably high followed by a post-yielding  
148 stage where the slope becomes flatter. While the interface capacity in the pre-yielding stage  
149 depends on the bond between the concrete topping and the hollowcore slab, the post-yielding  
150 behavior is governed by shear friction between the slab and the topping. Slabs A1 and A2 differ  
151 in the initial loading stage where slab A1 showed lower bond strength than slab A2. However,  
152 both slabs failed at similar loads. Slabs B1 and B2 had also failed at similar loads.

153

154 The abrupt failure type that was observed for all tested specimens emphasizes that the horizontal  
155 stress transferred along the interface layer did not have the ability to fully redistribute over the  
156 contact area once failure was initiated. This observation suggests that the reported values of  
157 average shear stresses are lower than the actual shear stresses that were reached.

158

## 159 **ANALYTICAL MODEL**

160 The hollowcore slabs are modeled as rigid elements. Two continuous spring systems were used  
161 to simulate the stiffness of the interface layer as illustrated in Fig. 8. Similar modeling technique  
162 was used by El Damatty and Abushagur<sup>7</sup> while modeling the adhesive attaching FRP sheets to

163 steel I beams. The first set of springs depicts the in-plane stiffness  $k_s$  in the direction of the  
 164 applied load (parallel to the X axis). They allow modeling the horizontal shear stress behavior.  
 165 The out-of-plane stiffness  $k_p$  models the peel behavior using another set of springs that are  
 166 parallel to the Z axis. The shear stress profile  $v_h(x)$  acting along the interface between the  
 167 hollowcore slab and the concrete topping can be calculated using Eq. 1, where  $u(x)$  is the in-  
 168 plane displacement profile of the concrete topping along the X axis.

169  $v_h(x) = k_s \times u(x)$  ..... (1)

170 In the following sections, in-plane and out-of-plane equilibrium analysis are conducted on an  
 171 infinitesimal segment of the concrete topping “element T” to evaluate the shear and peel  
 172 stiffnesses  $k_s$  and  $k_p$ .

173

174 **In-Plane Equilibrium**

175 When the hollowcore slab is pushed downward by the applied force  $P_{hc}$ , an equivalent reaction  
 176 force  $P_t$  is generated in the concrete topping as shown in Fig. 9. The resultant of the developed  
 177 axial stresses in the concrete topping,  $\sigma$ , is acting at its centroid.  $\sigma$  has a value of zero at the top  
 178 point of the topping ( $x = 0$ ) and a maximum value at the bottom point ( $x = 508$  mm).

179

180 Considering the in-plane equilibrium of an infinitesimal element T, the increase in axial stresses  
 181  $d\sigma$  is in equilibrium with the developed shear stresses at the interface. The force in the in-plane  
 182 spring,  $F_s$ , represents the shear force along the interface between the hollowcore slab and the  
 183 concrete topping. This force can be calculated from the summation of forces along the X axis as  
 184 given by Eq. 2.  $F_s$  can also be calculated as a function of the shear spring stiffness as given by  
 185 Eq. 3.

186  $F_s = d\sigma \times b \times t$  ..... (2)

187  $F_s = K_s \times u(x) \times b \times dx$  ..... (3)

188 The relationship between  $\sigma$  and the in-plane displacement  $u(x)$  can be obtained from Eqs. 2 and 3  
 189 and Hook's Law as illustrated in Eqs. 4 and 5.

190  $\frac{d\sigma}{dx} = k_s \times u(x) \times \frac{1}{t}$  ..... (4)

191  $\sigma = E_c \times \frac{du}{dx}$  .....

192 (5)

193 where  $(du / dx)$  is the strain in the concrete topping, and  $E_c$  is the modulus of elasticity of  
 194 concrete. Since the concrete topping is made of normal density concrete and have a compressive  
 195 strength  $f'_c$  of 30 MPa,  $E_c$  is calculated using clause 8.6.2.3 of CSA A23.3-4<sup>1</sup>. The differential  
 196 equation that governs the state of stresses in the concrete topping is:

197  $\frac{d^2u}{dx^2} - \omega^2 u(x) = 0$  ..... (6)

198 where  $\omega^2 = \left( \frac{k_s}{tE_c} \right)$  .....

199 (7)

200 Eq. 6 is a second order differential equation and can be solved by defining the following  
 201 boundary conditions:

202 (1) At  $x = 0 \rightarrow \frac{du}{dx} = 0$  (strain = 0)

203 (2) At  $x = L \rightarrow \frac{du}{dx} = -\frac{P_t}{btE_c}$  (strain from Hook's Law)

204 Solving Eq. 6 using the defined boundary conditions leads to the following in-plane  
 205 displacement profile.

$$206 \quad u(x) = -\frac{P_t}{btE_c\omega \sinh(\omega L)} \cosh(\omega x) \dots\dots\dots (8)$$

207 The relationship between the load  $P_t$  and the measured displacement at the bottom surface of the  
 208 concrete topping when  $x$  is equal to  $L$  can be expressed by Eq. 9.

$$209 \quad P_t = -btE_c\omega \tanh(\omega L)u(L) \dots\dots\dots (9)$$

210 where  $u(L)$  is the average in-plane displacement measured using LVDTs L3 and L4.

211  
 212 The measured  $P_t - u(x)$  is simplified to a bilinear curve as shown in Fig 10. The slope  $k_{sm}$  was  
 213 obtained such that areas A1 and A2 are equal. The coordinates of points C for all specimens are  
 214 reported in Table 2 and were used to define  $P_t$  and  $u(L)$  and then evaluate  $\omega$  using Eq. 9.

215  
 216 **Maximum Shear Stress ( $v_h \max$ )**

217 The in-plane displacement distribution along the X axis of the concrete topping can be obtained  
 218 using Eq. 8. The horizontal shear stress distribution,  $v_h$ , can be then evaluated using Eq. 1. Fig.  
 219 11 illustrates the horizontal shear stress distribution along the X axis. Fig. 12 compares the  
 220 calculated horizontal shear stress profile for slab B1 and the average measured horizontal shear  
 221 stress at failure. The actual horizontal shear profile shows a concentration of the shear stresses  
 222 near the applied load  $P_t$ . This observation indicates that the tested slabs sustained higher stresses  
 223 than the average value. Table 1 shows the average and the calculated horizontal shear stress  
 224 values at yielding. For all of the tested slabs, the shear strength at the interface between the

225 hollowcore slabs and the concrete topping reached values that are much higher than the values  
 226 specified in North American design standards.

227

228

229

230 **Out-of-Plane Equilibrium**

231 Fig. 9 illustrates the forces and stresses acting on element T in the out-of-plane direction. The  
 232 external applied moment,  $m(x)$ , results from the eccentric force in the shear spring,  $F_s$ , and can be  
 233 found by multiplying the force  $F_s$  by half the thickness of the concrete topping. The applied  
 234 moment,  $m(x)$ , can be defined using Eq. 10.

235 
$$m(x) = k_s \frac{bt}{2} u(x) \dots\dots\dots (10)$$

236 The force,  $F_p$ , is developed in the out-of-plane springs as a result of the applied moment  $m(x)$  and  
 237 is responsible for the peel behavior of the concrete topping.  $F_p$  can be calculated from the  
 238 equilibrium of forces along the Z axis and the equilibrium of the external and the internal  
 239 moments acting on the element, Eqs. 11 and 12.

240 
$$\frac{dV}{dx} = -k_p bw(x) \dots\dots\dots (11)$$

241 
$$\frac{dM}{dx} = V + m(x) \dots\dots\dots (12)$$

242 Utilizing the moment-curvature relationship, Eq. 13, the differential equation governing the peel  
 243 behavior, Eq. 14, can be derived.

244 
$$M(x) = EI \frac{d^2 w}{dx^2} (x) \dots\dots\dots (13)$$

245 
$$\frac{d^4 w(x)}{dx^4} + \lambda^4 w(x) = \frac{1}{EI} \frac{dm}{dx}$$

246 ..... (14a)

247 where  $\lambda^4 = \frac{bk_p}{EI}$  ..... (14b)

248

249 The homogenous and particular solutions of Eq. 14 are given by Eq. 15.

250  $w(x) = A \cos(\lambda x) \cosh(\lambda x) + B \cos(\lambda x) \sinh(\lambda x)$   
251  $+ C \sin(\lambda x) \cosh(\lambda x) + D \sin(\lambda x) \sinh(\lambda x) \cos(\lambda x) - F \sinh(\omega x)$  ..... (15a)

251 where  $F = \frac{P_t k_s}{E_c^2 I \sinh(\omega L) (\lambda^4 + \omega^4)}$  .....

252 (15b)

253 The constants  $B$  and  $D$  can be determined by applying the following boundary conditions at the  
254 free end of the concrete topping ( $x = 0$ ).

255 (1)  $\frac{d^2 w}{dx^2} = 0$  ( $M = 0$ ).

256 (2)  $\frac{d^3 w}{dx^3} = 0$  ( $V = 0$ ).

257

258 Substituting with the evaluated constants, Eq. 15 reduces to the following form:

259  $w(x) = A \cos(\lambda x) \cosh(\lambda x) + C[\cos(\lambda x) \sinh(\lambda x) + \sin(\lambda x) \cosh(\lambda x)]$   
260  $+ \frac{F}{2} \frac{\omega}{\lambda} \cos(\lambda x) \sinh(\lambda x) + F \sinh(\omega x)$  ..... (16)

260

261 Eq. 16 represents the calculated out-of-plane displacement profile of the concrete topping,  $w(x)$ ,  
262 and contains three unknowns  $A$ ,  $C$  and  $\lambda$ . The load and displacement defining point C in Fig. 10  
263 and the corresponding strains (point D in Fig. 13) are used to evaluate these constants as follows:

- 264 1- The values of  $(du/dx)_{mid}$ , Fig. 14, are evaluated at the locations of S1, S3 and S5 by  
 265 differentiating Eq. 8.
- 266 2- Readings of S1, S3, and S5 represent the measured strain at the surface of the concrete  
 267 topping,  $(du/dx)_{outer}$ , Fig. 14.
- 268 3-  $(du/dx)_{bending}$  is evaluated at the locations of S1, S3, and S5 using Eq. 17.

269 
$$\left(\frac{du}{dx}\right)_{bending} = \left(\frac{du}{dx}\right)_{outer} - \left(\frac{du}{dx}\right)_{mid} \dots\dots\dots (17)$$

- 270 4- The curvature of the concrete topping at the locations of S1, S3 and S5 is evaluated using  
 271 Eq. 18.

272 
$$\left(\frac{d^2w}{dx^2}\right) = -\frac{2}{t}\left(\frac{du}{dx}\right)_{bending} \dots\dots\dots (18)$$

- 273 5- The cubic function that best fits the calculated curvature in step 4 is then evaluated. Fig.  
 274 15 shows a typical cubic function.
- 275 6- The out-of-plane measured displacement profile  $w(x)_m$  was obtained by double  
 276 integration of Eq. 18. The two integration constants were then evaluated using the out-of-  
 277 plane displacement readings from LVDTs L1 and L2.
- 278 7- Nonlinear regression analysis was conducted to match the calculated out-of-plane  
 279 displacement profile  $w(x)$  with the displacement profile  $w(x)_m$  evaluated in step 6. This  
 280 analysis allowed determining constants  $A$ ,  $C$  and  $\lambda$ .

281

282 **Shear and Peel Stiffnesses**

283 The peel stiffness  $k_p$  is calculated using Eq. 14b by substituting with the value of  $\lambda$ . The out-of-  
 284 plane profile,  $w(x)$ , is shown in Fig. 16 for all tested slabs. The shear stiffness  $k_s$  is calculated

285 using Eq. 7. Table 3 presents the calculated shear and peel stiffnesses for all slab specimens.  $k_p$  is  
286 considerably smaller than  $k_s$  for all slabs. Average shear stiffnesses ( $k_s$ ) of 50.8 (N/mm)/mm<sup>2</sup> and  
287 6.8 (N/mm)/mm<sup>2</sup> and peel stiffnesses ( $k_p$ ) of 7.2 (N/mm)/mm<sup>2</sup> and 2.0 (N/mm)/mm<sup>2</sup> were  
288 calculated for slabs from manufacturer A and B, respectively. Manufacturers A and B can use  
289 these values to predict the composite behavior of their hollowcore slabs.

290

## 291 **SUMMARY AND CONCLUSIONS**

292 Push-off tests that examine the shear and peel behavior at the interface between four hollowcore  
293 slabs and their concrete topping were presented in this paper. All of the slabs had a lightly-  
294 roughened surface finish using a conventional steel broom and achieved slightly higher average  
295 shear stresses than required by the North American design standards. Comparing the average  
296 shear results indicated that the shear strength considerably varies between hollowcore slabs from  
297 different manufacturers. An analytical model that simulates the interface between the hollowcore  
298 slab and the concrete topping using continuous springs was utilized. The springs depicted the  
299 interfacial shear and peel behaviors. The actual shear stresses were evaluated using the analytical  
300 model and found to be higher than the average measured values for all of the tested slabs. The  
301 actual values are much higher than the specified code limits. The shear and peel stiffnesses,  $k_s$   
302 and  $k_p$ , of the interface between hollowcore slabs and concrete topping were then estimated using  
303 the presented analytical model. The reported  $k_s$  and  $k_p$  values are unique for the tested slabs. The  
304 presented method can be repeated to evaluate these stiffnesses for slabs from different  
305 manufacturers. Structural engineers can then use  $k_s$  and  $k_p$  values to evaluate the actual shear  
306 stresses developed at the interface between hollowcore slabs and their concrete topping and  
307 judge on the appropriateness of using the composite action.

308

309

310 **5. ACKNOWLEDGMENTS**

311 The authors would like to acknowledge the enthusiastic guidance and advice provided by Mr.  
312 Anil Mehta from The Prestressed Group (Windsor, ON). Appreciation is extended to the  
313 Canadian Precast/Prestressed Institute (CPCI) and the Ontario Centers of Excellence (OCE) for  
314 their financial and technical support.

315

316 **REFERENCES**

- 317 1. CSA A23.3-04 (2004). "Design of concrete structures." *Canadian Standard Association*,  
318 Mississauga, Canada.
- 319 2. ACI 318-08 (2008). "Building Code Requirements for Structural Concrete (ACI 318-08) and  
320 Commentary." *American Concrete Institute*, Michigan, United States.
- 321 3. Technical Bulletin 74-B6 (1974). "Composite Systems Without roughness." *Concrete*  
322 *Technology Association (CTA)*, CTA 35, pp 271-316.
- 323 4. Technical Bulletin 76-B4 (1976). "Composite Systems without Ties." *Concrete Technology*  
324 *Association (CTA)*, CTA 36, pp 317-360.
- 325 5. Girhammar U.A. and Pajari M. (2008). "Tests and analysis on shear strength of composite  
326 slabs of hollow core units and concrete topping." *Construction and Building Materials*, 22,  
327 1708-1722.
- 328 6. Ibrahim I. S. and Elliot K. S. (2006). "Interface Shear Stress of Hollow Core Slabs with  
329 Concrete Toppings." *Sixth International Conference on Concrete Engineering and*  
330 *Technology, (CONCET 2006)*, Institution of Engineers Malaysia, Kuala Lumpur, 104-116
- 331 7. El Damatty A.A. and Abushagur M. (2003). "Testing and modeling of shear and peel  
332 behavior for bonded steel/FRP connections." *Thin-Walled Structures*, 41, 987-1003.

- 333 8. CSA A23.1-09 (2009). “Concrete materials and methods of concrete construction.”  
334 *Canadian Standard Association*, Mississauga, Canada.
- 335 9. ASTM C349, (2008), “Standard Test Method for Compressive Strength of Hydraulic-Cement  
336 Mortars”, *ASTM International*, Pennsylvania, United States.
- 337 10. ASTM C39/C39M, (2005), “Standard Test Method for Compressive Strength of Cylindrical  
338 Concrete Specimens”, *ASTM International*, Pennsylvania, United States.
- 339

340 **NOTATIONS**

341

342 **b**: width of the concrete topping in the push-off tests, 508 mm

343  $E_c$ : modulus of elasticity of concrete

344  $f'_c$ : concrete compressive strength

345  $F_s$ : in-plane force on element T in the X direction

346  $F_p$ : out-of-plane force on element T

347  $k_p$ : peel stiffness at the interface between the hollowcore slab and the concrete topping

348  $k_s$ : shear stiffness at the interface between the hollowcore slab and the concrete topping

349  $k_{sm}$ : slope of the measured load-displacement graph

350 **L**: length of the concrete topping in the push-off tests, 508 mm

351 **M**: internal moment in the concrete topping

352  $m(x)$ : external applied moment on the concrete topping

353  $P_{hc}$ : load applied on the hollowcore slab using the hydraulic actuator during the push-off test

354  $P_p$ : load at the end of the linear stage, determined from the load-strain graphs

355  $P_r$ : reaction on the concrete topping during the push-off tests

356 **t**: concrete topping thickness in the push-off tests, 50 mm

357  $u(x)$ : in-plane displacement profile along the axis X

358 **V**: internal shear force in the concrete topping

359  $w(x)$ : calculated out-of-plane displacement profile of the concrete topping

360  $w(x)_m$ : measured out-of-plane displacement profile of the concrete topping

361  $\nu_h$ : shear stress

362  $\nu_{h\ avg.}$ : average measured shear stress

363  $\nu_{h\ max.}$ : maximum shear stress calculated using the analytical model

364 Table 1: Push-off test results

<b>Specimen</b>	<b>Failure load,</b>	<b>Measured average shear</b>	<b>Calculated yielding</b>
<b>Label</b>	<b>kN</b>	<b>strength, <math>v_h</math> avg.,</b>	<b>horizontal shear stress,</b>
		<b>MPa</b>	<b><math>v_h</math> max., MPa</b>
<b>A1</b>	504	1.95	6.19
<b>A2</b>	554	2.15	7.24
<b>B1</b>	223	0.86	1.24
<b>B2</b>	182	0.71	1.01

365

366 Table 2: Values of  $P_i$  and  $u(L)$  at the yielding points, C

<b>Slab label</b>	<b><math>P_i</math>, kN</b>	<b><math>u(L)</math>, mm</b>
<b>A1</b>	504	0.130
<b>A2</b>	554	0.134
<b>B1</b>	223	0.184
<b>B2</b>	182	0.148

367

368 Table 3: Shear and Peel stiffnesses

<b>Specimen</b>	<b>Horizontal shear stiffness <math>k_s</math>, (N/mm)/mm<sup>2</sup></b>	<b>Peel stiffness <math>k_p</math>, (N/mm)/mm<sup>2</sup></b>
<b>A1</b>	47.60	3.82
<b>A2</b>	54.00	2.96
<b>B1</b>	6.72	0.80
<b>B2</b>	6.85	1.06

369

370 **LIST OF TABLES**

371 Table 1: Push-off test results

372 Table 2: Values of  $P_t$  and  $u(L)$  at the yielding points, C

373 Table 3: Shear and Peel stiffnesses

374

375



376



377



378

379 Fig. 1: Lightly roughened hollowcore slabs,

380 a. Roughening method, b. Manufacturer A pattern, c. Manufacturer B pattern

381



382

383 Fig. 2: 50 mm cubes for compressive strength test

384

385



386



387

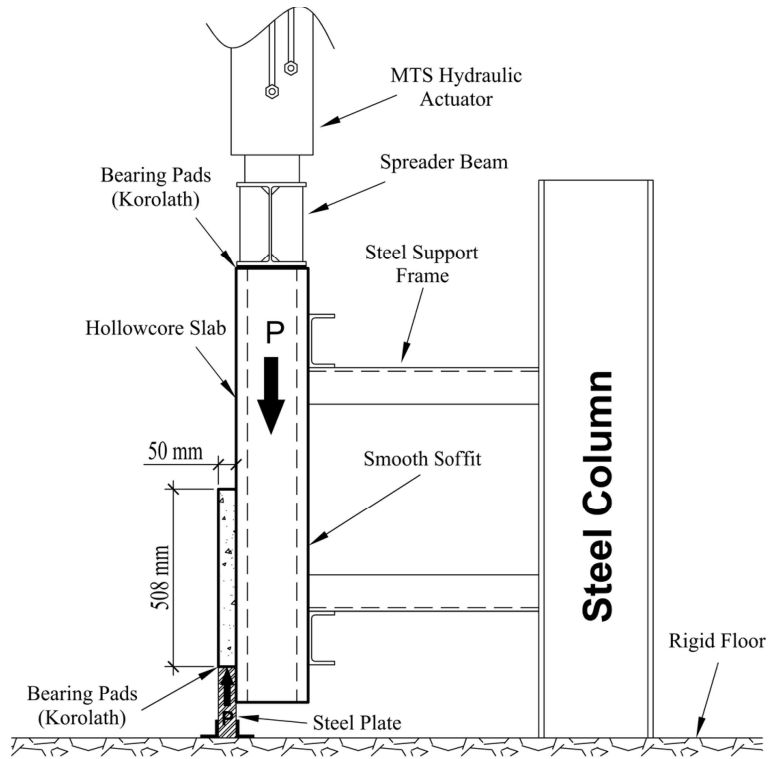
388 Fig. 3: Concrete topping

389 a. Formwork of concrete topping

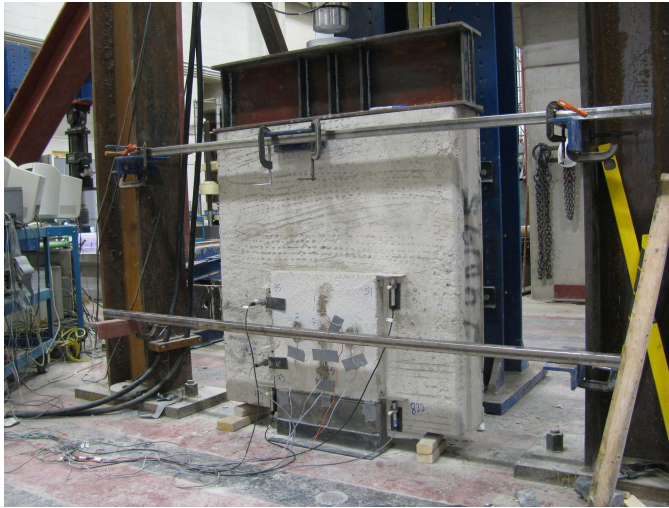
390 b. Casting of concrete topping

391

392



393

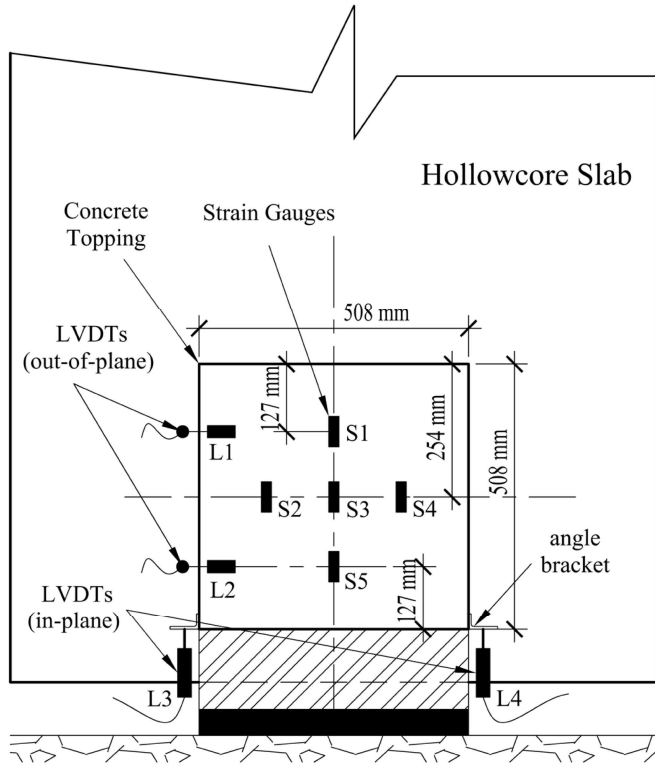


394 Fig. 4: Push-off test setup

395 a. Schematic

396 b. Photo

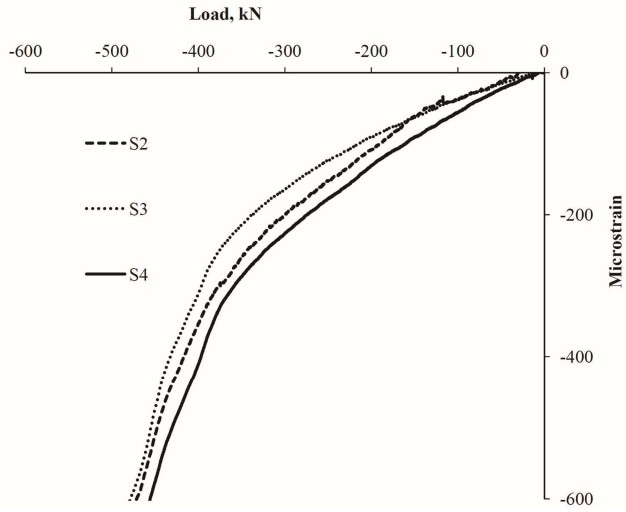
397



398

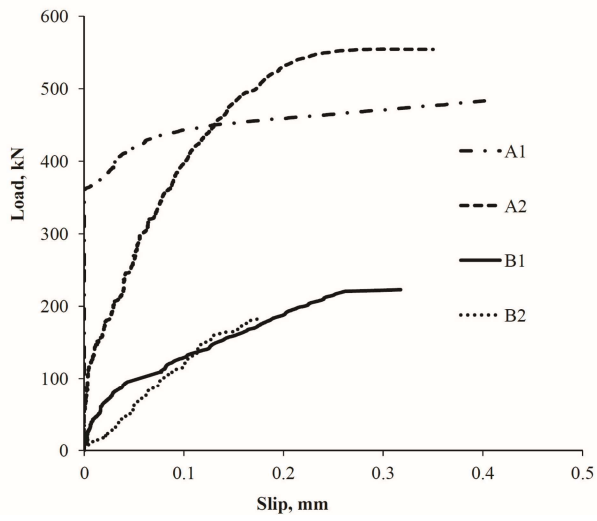
399 Fig. 5: Instrumentation

400



401

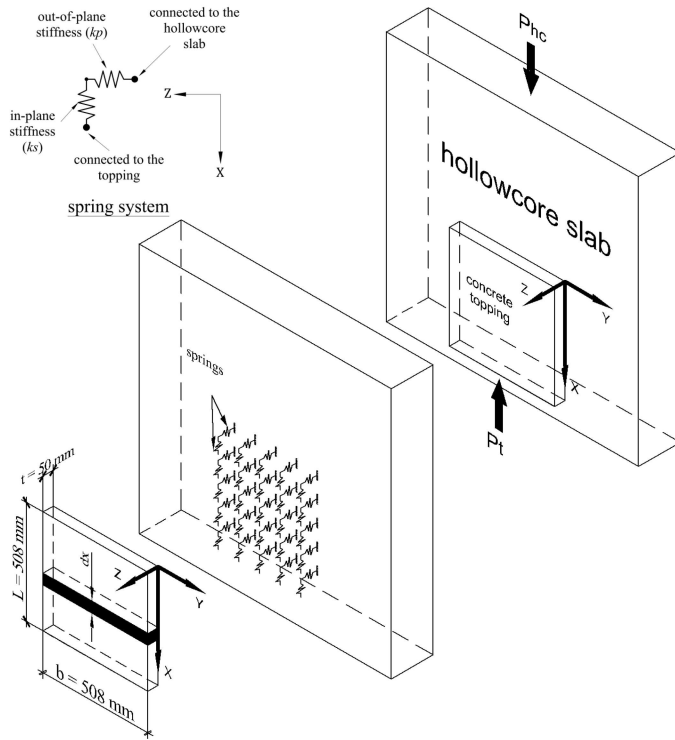
402 Fig. 6: Strain gauge readings for slab A1



403

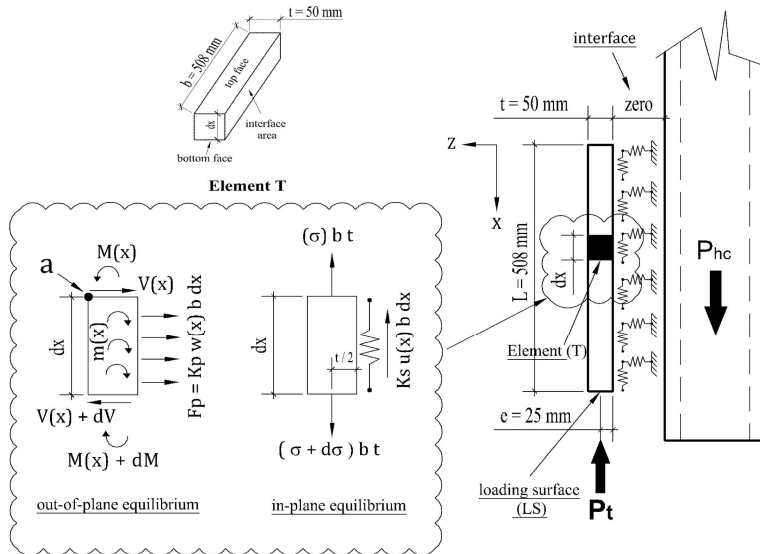
404 Fig. 7: Load-slip curves

405



406

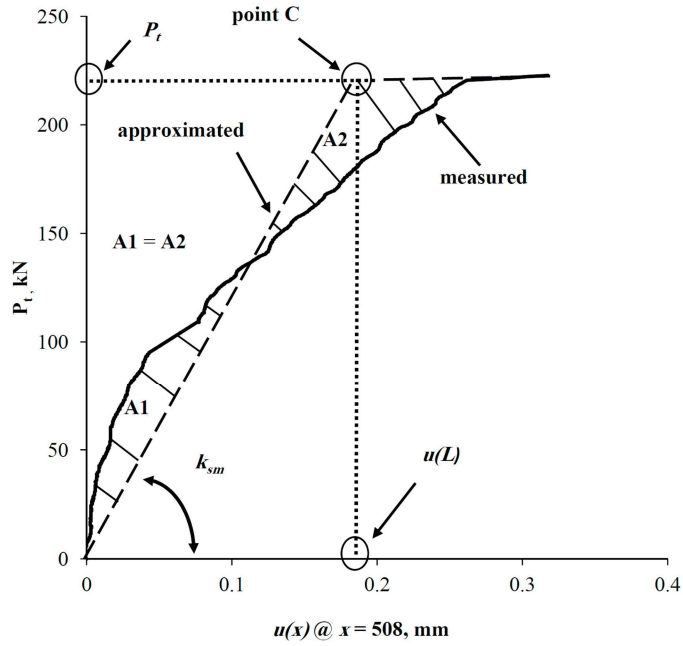
407 Fig. 8: General layout of the push-off test spring model



408

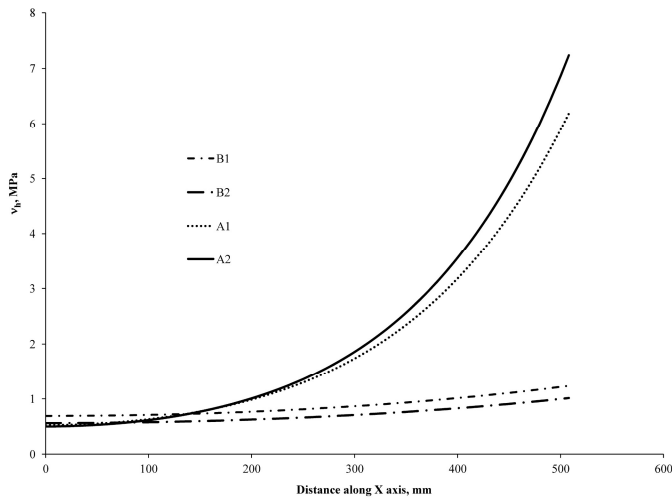
409 Fig. 9: Free body diagram of element T showing in-plane equilibrium

410



411

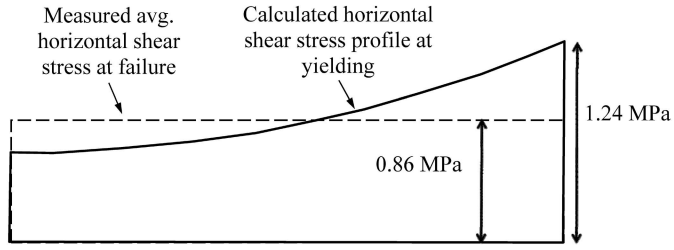
412 Fig. 10: Approximate load-slip relationship for slab B1 (typical)



413

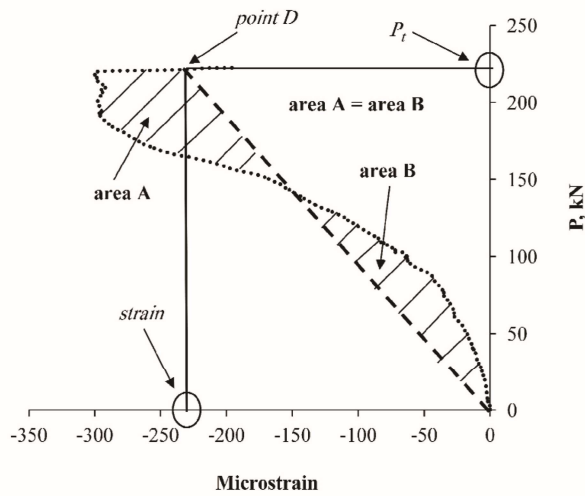
414 Fig. 11: Horizontal shear stress distribution

415



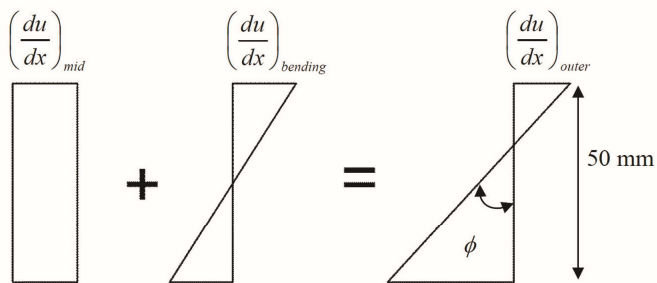
416

417 Fig. 12: Horizontal shear stress distribution for slab B1 (typical)



418

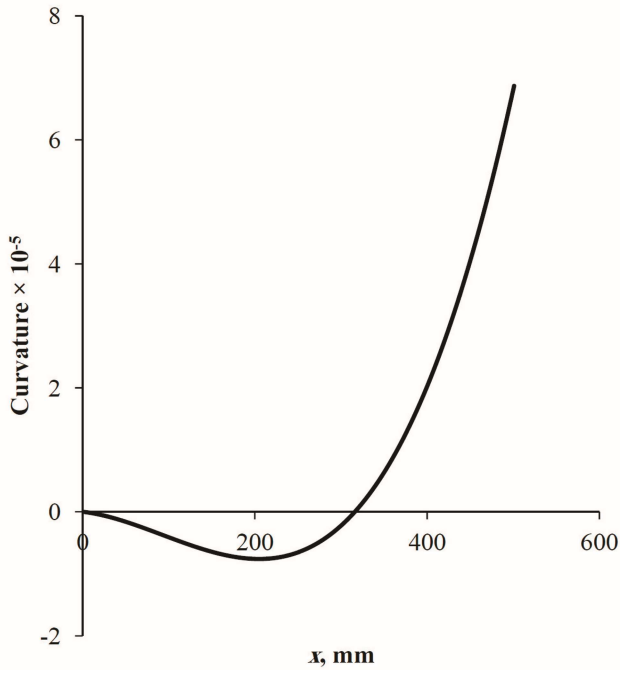
419 Fig. 13: Approximate load-S3 strain relationship for slab B1 (typical)



420

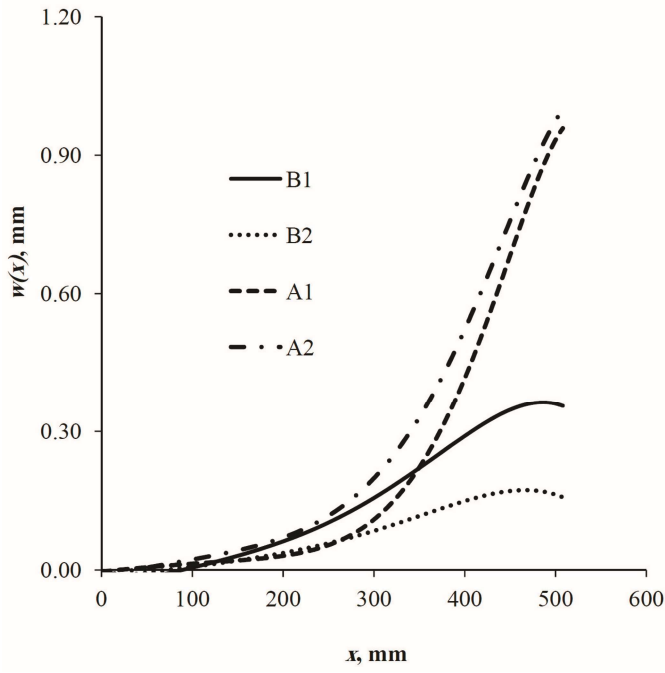
421 Fig. 14: State of strains in the concrete topping

422



423

424 Fig. 15: Curvature best fit cubic curve



425

426 Fig. 16: Out-of-plane displacement profiles

427

428